Conformational Analysis and Receptor Docking of *N*-[(1*S*,2*S*)-3-(4-Chlorophenyl)-2-(3-cyanophenyl)-1-methylpropyl]-2-methyl-2-{[5-(trifluoromethyl)pyridin-2-yl]oxy}propanamide (Taranabant, MK-0364), a Novel, Acyclic Cannabinoid-1 Receptor Inverse Agonist

Linus S. Lin,*,# Sookhee Ha,† Richard G. Ball,‡ Nancy N. Tsou,‡ Laurie A. Castonguay,† George A. Doss,# Tung M. Fong,§ Chun-Pyn Shen,§ Jing Chen Xiao,§ Mark T. Goulet,# and William K. Hagmann#

Departments of Medicinal Chemistry, Molecular Systems, Process Research, and Metabolic Disorders, Merck Research Laboratories, Rahway, New Jersey 07065

Received November 30, 2007

X-ray crystallographic, NMR spectroscopic, and computational studies of taranabant afforded similar low-energy conformers with a significant degree of rigidity along the C11−N13−C14−C16−C17 backbone but with more flexibility around bonds C8−C11 and C8−O7. Mutagenesis and docking studies suggested that taranabant and rimonabant shared the same general binding area of CB1R but with significant differences in detailed interactions. Similar to rimonabant, taranabant interacted with a cluster of aromatic residues (F(3.36)200, W(5.43)279, W(6.48)356, and Y(5.39)275) through the two phenyl rings and with F(2.57)170 and L(7.42)387 through the CF_3−Pyr ring. The notable distinction between taranabant and rimonabant was that taranabant was hydrogen-bonded with S(7.39)383 but not with K(3.28)192, while rimonabant was hydrogen-bonded with K(3.28)192 but not with S(7.39)383. The strong hydrogen bonding between the amide NH of taranabant and hydroxyl of S(7.39)383 was key to the superior affinity of taranabant to CB1R.

Introduction

The rich pharmacology of cannabinoids and their receptors has been a subject of research for decades. Of particular interest in recent years is the role of cannabinoid-1 receptor (CB1R[a]) in regulating energy homeostasis. Marijuana use is known to be associated with increased appetite in humans, and this pharmacological effect is believed to be mediated through activation of CB1R.[1] Conversely, CB1R inverse agonists have been shown to inhibit food intake in animals and humans.[2] In addition, CB1R inverse agonists are shown to increase energy expenditure.[3] Upon chronic administration of CB1R inverse agonists, weight loss has been observed in rodents and in humans.[4]

Rimonabant is the first CB1R inverse agonist that has undergone clinical evaluations for the treatment of obesity.[4b] Numerous structurally related CB1R inverse agonists, including SLV319, have since been reported, many of which share a cyclic core.[5,9] Recently, we disclosed a structurally distinct CB1R inverse agonist (taranabant, MK-0364) that is in the late stages of clinical evaluations for the treatment of obesity (Figure 1).[6,7] Unlike rimonabant or SLV319, taranabant lacks a rigid cyclic core and may be reasonably expected to have a high degree of structural flexibility. In this paper, we report X-ray crystallographic, NMR spectroscopic, and computational studies that suggest taranabant is structurally more rigid than was anticipated. Molecular modeling, mutagenesis, and receptor docking studies suggest that the bioactive conformation of taranabant has significant overlap with that of rimonabant, and the two classes of inverse agonists share a similar binding area of CB1R, although they differ notably in detailed interactions.

Results and Discussion

Our structural analysis of taranabant started with the determination of its X-ray crystal structure which revealed two crystallographically independent molecules in one unit cell of the crystal lattice. The two molecules had only minor differences in their conformations except for a twist of the cyanophenyl ring of about 144°. A perspective view of one of the molecules is shown in Figure 2 with selected dihedral angles listed in Table 1. Further examination of the solid state conformation of taranabant uncovered three pairs of substituents with *anti*-arrangements around the two consecutive bonds: C14−C16 and C16−C17, setting up two pairs of antiperiplanarly disposed hydrogens, H*a*/H*b* and H*b*/H*d* (Table 1). The overall result was a perfect staggering of all substituents on the C14−C16−C17 skeleton of taranabant, thereby avoiding any potential eclipsing or *syn*-pentane interactions. Also noteworthy was the *anti*-orientation between H*a* and H*q*, which precluded gauche interactions between C11 and C16 or C11 and C15. Examination of similar structures in the Cambridge Structural Database (12 reference codes, 19 observations) afforded a narrow range of values, ±160–180°, for the torsion angle equivalent to H*a*−C14−N13−H*q*, which suggested a strong preference for the hydrogen atom on C14 to lie in the amide plane and reflected a certain restriction of rotation about the N13−C14 bond. The crystal structure also featured a *trans*-amide bond, placing C8 and C14 at a dihedral angle of –172.8°. Finally, the 5-CF_3-Pyr ring was folded over the 4-Cl-Ph ring and may be positioned for edge-to-edge π-interactions (distance between C2 and C19, 3.5 Å).

Intrigued by the conformational preference in the solid state, we proceeded to study the solution conformation of taranabant. First, 1D ^{1}H NMR and 2D ^{1}H−^{13}C HSQC NMR spectra were recorded in CD_3OD to allow complete assignment of the proton signals. The coupling constants were extracted with a selected

* To whom correspondence should be addressed. Phone: 732-594-8391. Fax: 732-594-5966. E-mail: linus_lin@merck.com.
† Molecular Systems.
‡ Process Research.
§ Metabolic Disorders.
# Medicinal Chemistry.

[a] Abbreviations: CB1R, cannabinoid-1 receptor; bRho, bovine rhodopsin; EC, extracellular; IC, intracellular; TM, transmembrane; WT, wild type; CHO, Chinese hamster ovary; GPCR, G-protein coupled receptor.

10.1021/jm7014974 CCC: $40.75
Published on Web 03/12/2008

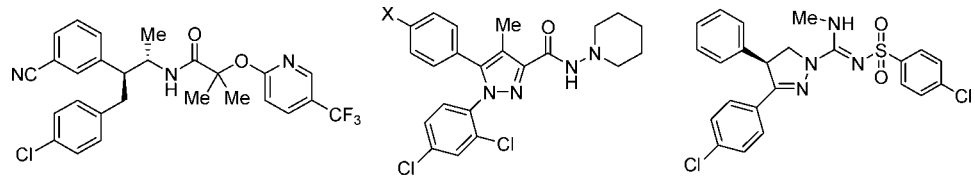

Taranabant (MK-0364) **X = Cl: Rimonabant (SR141716A)** **X = I: AM251** **SLV319**

Figure 1. Selected structures of CB1R inverse agonists.

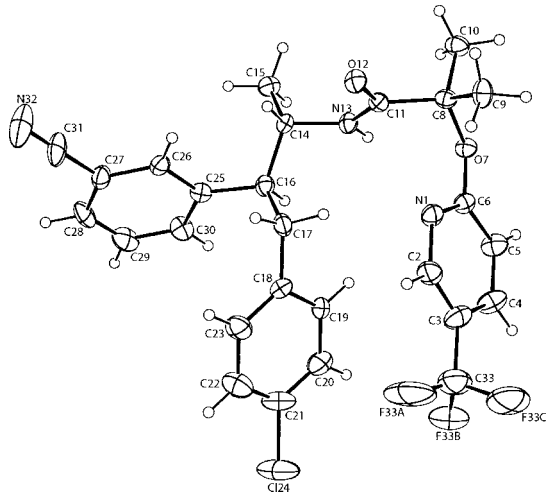

Figure 2. An ORTEP representation of one of the two independent molecules of taranabant. Ellipsoids are 50%, H atoms are arbitrary spheres.

Table 1. Selected Dihedral Angles of X-ray Structure of Taranabant

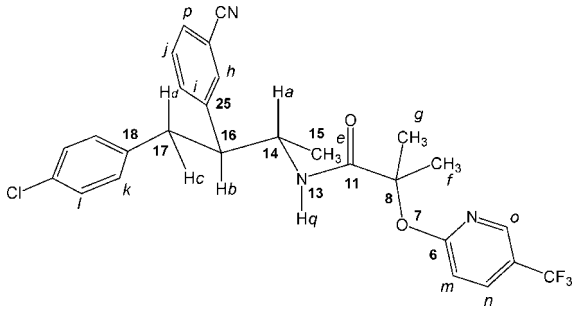

torsional angles	deg
C14−C16−C17−C18	−161.4
N13−C14−C16−C25	−177.5
C15−C14−C16−C17	179.3
H*b*−C16−C17−H*d*	−165.1
H*a*−C14−C16−H*b*	−176.6
H*a*−C14−N13−H*q*	179.3
C8−C11−N13−C14	−172.8
C6−O7−C8−C11	−67.6
O7−C8−C11−N13	−34.4

subset listed in Table 2. Most noteworthy were the large coupling constants for H*a*/H*b*, H*b*/H*d*, and H*a*/H*q*, consistent with antiperiplanar arrangement of these three pairs of hydrogens. A 2D ^{1}H−^{1}H NOESY study was also carried out (Figure 3) to gain additional insights in the solution conformation of taranabant. Key NOEs are summarized in Table 3. The strong NOEs observed for H*a*/H*d*, H*d*/H*h*, and H*d*/H*i* and the large coupling constant between H*b* and H*d* were consistent with the staggered arrangement, as observed in the solid state, with the two phenyl rings gauche to each other and with H*c* and H*d*

Table 2. Selected Coupling Constants of Taranabant in CD_3OD

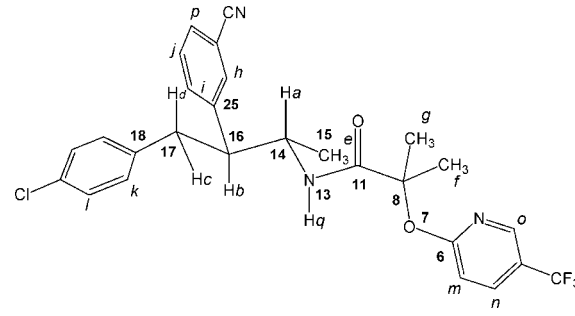

pair of hydrogens	*J* (Hz)
H*a*/H*b*	10.1
H*b*/H*d*	11.7
H*c*/H*d*	13.8
H*a*/H*q*	9.0
H*b*/H*c*	3.7

occupying the pseudo axial and pseudo equatorial position, respectively. The NOE observed for H*a*/H*c* and lack of NOEs for H*c*/H*h* or H*c*/H*i* and a medium coupling constant between H*b* and H*c* were all consistent with such a conformation.

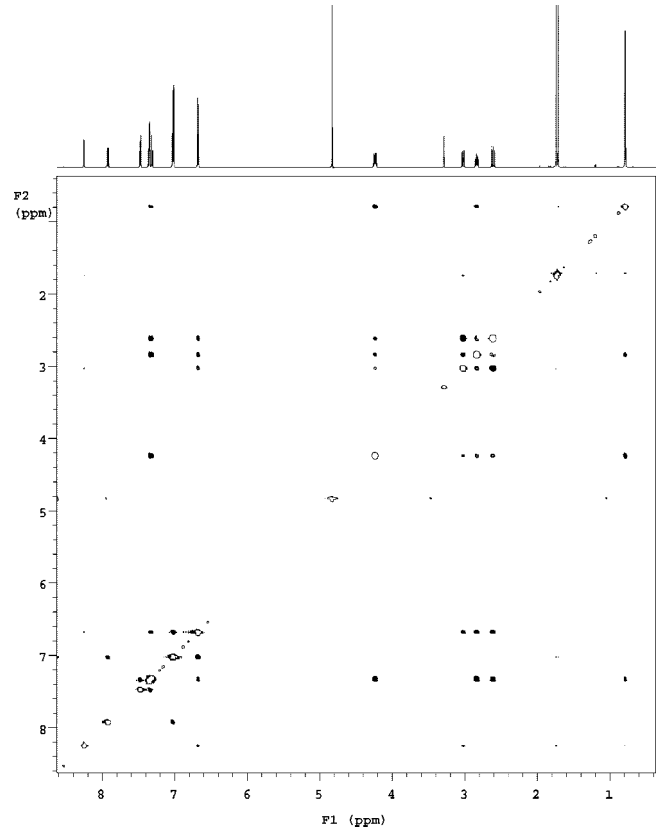

Figure 3. NOESY spectrum of taranabant in methanol-d_4.

Table 3. Key NOEs of Taranabant Observed in CD_3OD

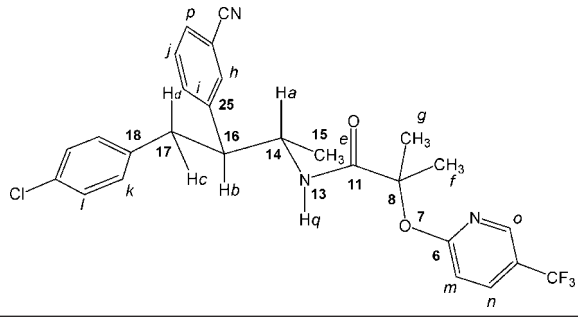

pairs with strong NOEs	pairs with medium NOEs	pairs with weak NOEs	NOE not observed for pairs
H*b*/H*e*, H*h*, H*i*, H*d* /H*a*, H*h*, H*i* H*f*, H*g*/H*m*	H*a*/H*c*	H*c*, H*e*, H*f*, H*g*, H*k*/H*o* H*f*/H*c*, H*h*, H*k* H*a*, H*h*, H*i*/H*k*	H*c*/H*h*, H*i* H*e*/H*m* H*g*/K*c*, K*h*, H*k*

However, weak NOEs observed for H*f*/H*k* and H*k*/H*o* could not be explained by the above conformer but can be rationalized by another conformer with a 120° rotation of the C16—C17 bond, thus allowing a shorter distance between the Cl-Ph ring and the CF_3-Pyr ring. Because only a weak NOE was observed for H*a*/H*k*, the latter conformer was unlikely to account for a significant population. In addition, NOEs for both H*c*/H*o* and H*e*/H*o* could not be readily explained with a single conformer, and multiple conformers may exist with the CF_3-Pyr ring residing on either side of the amide plane. Such rotational freedom around C8−C11 and O7−C8 was also supported by weak NOEs observed for H*c*/H*f* and H*f*/H*h*.

Computational studies were then performed to further understand the molecular geometry and energetics of taranabant. Over 80 unique conformers were generated with energies ranging within 12 kcal/mol. Perhaps, this result should not be surprising considering the large number of rotatable bonds (total of eight). However, closer examination revealed that the structural variation was largely associated with the carboxyl portion of the molecule, while only limited permutations were found with the rest of the molecule. Representative conformers are listed in Figure 4. First, conformer A, which was found to possess the lowest energy, was virtually identical to the X-ray crystal structure. As discussed earlier, this conformation featured staggered arrangement of substituents around bond C14−C16 and C16−C17, a *trans*-amide bond, and the CF_3-Pyr ring folded over the 4-Cl-Ph ring. Rotation of 120° around the C16−C17 bond afforded conformer C with 2.8 kcal/mol increase in energy, consistent with the notion that such a conformation would account for only a small population in solution. Conformational freedom around the C8−C11 bond was evident with conformer B, where the CF_3-Pyr ring rotated to the other side of the amide plane with only a slight increase in energy. Rotation of the C8−O7 bond of conformer A resulted in conformer D, with an increase of 3.6 kcal/mol in energy, presumably because of loss of $\pi-\pi$ interactions between the CF_3-Pyr and Cl-Ph ring and additional gauche interactions between the CF_3-Pyr ring and the methyl groups.

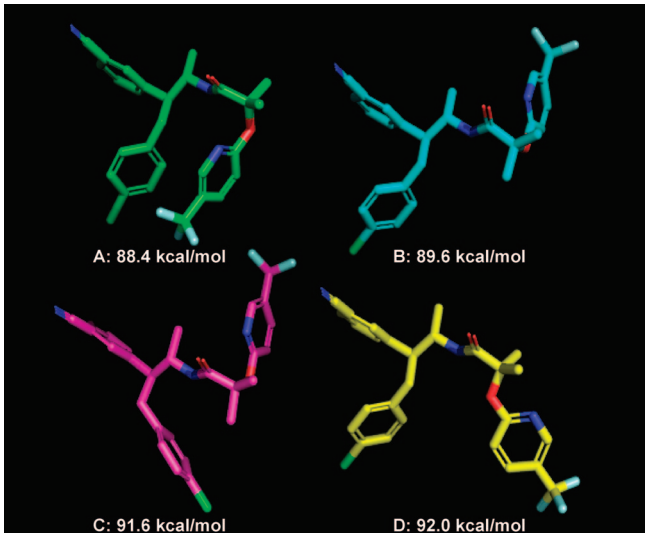

Figure 4. Representative conformers of taranabant generated from molecular mechanical calculations.

In summary, X-ray crystallographic, solution NMR, and computational studies of taranabant afforded similar low-energy conformers with a significant degree of rigidity, particularly around bond C11−N13, N13−C14, C14−C16, and C16−C17. With the exception for the amide bond (C11−N13), the structural rigidity was enforced with nonbonded interactions to minimize gauche or eclipsing arrangement. In contrast, rotations around bond C7−C11 and O7−C8 were more flexible, allowing the CF_3-Pyr ring pointing to various directions.

The binding mode of rimonabant to CB1R has been studied extensively through SAR, mutagenesis, and molecular modeling.[8] Two key features have been highlighted: (1) an aromatic cluster formed by F3.25(190), F3.36(200), W4.64(255), W5.43(279), W6.48(356), and Y5.39(275) that is in contact with the two phenyl rings of rimonabant through a series of aromatic stacking interactions;[8c] (2) K3.28(192) that forms a hydrogen bond with the amide carbonyl oxygen of rimonabant. This interaction was proposed to be key to the stabilization of the putative inactive state of CB1R.[8b,d] S7.39(383), which resides across from K3.28(192) in the active site, appears to have no direct interaction with rimonabant.[8a]

To determine whether taranabant binds to a similar pocket of CB1R as rimonabant, we constructed five human CB1R mutant receptors: F3.36(200)L, W5.43(279)A, K3.28(192)L, S7.39(383)A, and F(2.57)170L. The affinity of taranabant to the wild type and mutant receptors was assessed by competitive binding with [^{3}H]-CP55940 (Table 4). In the case of mutant receptor S7.39(383)A, the binding of CP55940 was dramatically diminished, and [^{3}H]-SR141716 was used as the radiolabeled ligand instead. The affinity of AM251, a close analogue of rimonabant, was also determined, and the IC_{50} values were compared with the reported values of rimonabant. First, the binding of AM251 was affected substantially by both W5.43(279)A (54-fold) and K3.28(192)L (17-fold) mutations, while a more modest reduction in affinity was observed for binding to the F3.36(200)L (9-fold) mutant receptor. In contrast, the S7.39(383)A (2-fold) mutation had little effect on the binding of AM251. These results were consistent with the reported data of rimonabant (Table 4).[8] The F2.57(170)L mutant receptor has not been reported in the literature, and we found for the first time that the binding of AM251 was dramatically impacted by this mutation (97-fold). Lange et al. had proposed based on docking studies that the piperidine ring of rimonabant may have hydrophobic contacts with F(2.57)170, and the right-hand 4-Cl-Ph ring of SLV319 may be engaged in π-stacking interactions with F(2.57)170.[9] Similar to AM251, the binding of taranabant was also affected by W5.43(279)A (7-fold), F3.36(200)L (7-fold), and F(2.57)170L (30-fold) mutations. It is interesting to note that the W5.43(279)A mutation impacted the binding of rimonabant (>1000-fold) more than AM251 (54-fold) and

Table 4. Binding of Taranabant and AM251 to Wild Type and Selected Mutants of Human CB1R

	WT	F200L	W279A	K192L	S383A	F170L
taranabant, IC_{50}, nM (fold change[a])	0.74 ± 0.29	5.0 ± 0.92 (7)	4.9 ± 1.2 (7)	1.2 ± 0.057 (2)	19 ± 5.7 (202)[b]	22 ± 0.042 (30)
AM251 IC_{50}, nM (fold change[a])	3.5 ± 0.068	30 ± 7.5 (9)	190 ± 0.5 (54)	60 ± 10 (17)	0.59 ± 0.25 (2)[b]	340 ± 97 (97)
rimonabant (fold change[a])		(3)[8c,c]	(>1000)[8c]	(17)[8b]	(<2)[8a]	

[a] IC_{50} on WT and mutant CB1R was determined with ^{3}H-CP55940 as the radio ligand except otherwise noted; the fold change was calculated by dividing the IC_{50} value on the mutant by the IC_{50} value on the WT. [b] ^{3}H-SR141716A was used as the radio ligand; IC_{50} of taranabant and AM251 on the WT CB1R is 0.094 ± 0.006 and 0.32 ± 0.03, respectively. [c] IC_{50} of rimonabant was obtained from the F200A mutant.

```
                EC1                                          TM1
bRho    MNGTEGPNFY VPFSNKTGVV RSPFEAPQYY LAEPWQFSML AAYMFLLIML
hCb1R   ---------- ---------- --------FM VLNPSQQLAI AVLSLTLGTF

                           IC1   TM2
GFPINFLTLY VTVQHKKLRT -PLNYILLNL AVADLFMVFG GFTTTLYTSL
TVLENLLVLC VILHSRSLRC RPSYHFIGSL AVADLLGSVI FVYSFIDFHV

 EC2 TM3                                      IC2
HGYFVFGPTG CNLEGFFATL GGEIALWSLV VLAIERYVVV CKPMSNFRFG
F-HRKDSRNV FLFKLGGVTA SFTASVGSLF LTAIDRYISI HRPLAYKRIV

 TM4                                EC3                TM5
-ENHAIMGVA FTWVMALACA APPLVGWSRY IPEGMQCSCG IDYYTPHEET
TRPKAVVAFC LMWTIAIVIA VLPLLGWNC- --EKLQSVCS -DIF-PHIDE
                                  IC3
NNESFVIYMF VVHFIIPLIV IFFCYGQLVF TVKEAAAAT- ----------
TYLMFWIGVT SVLLLFIVYA YMYILWKAHS HAVRMIQRGT QKSIIIHTSE

                TM6                                    EC4
---------- TQKAEKEVTR MVIIMVIAFL ICWLPYAGVA FYIFTHQGSD
DGKVQVTRPD QARMDIRLAK TLVLILVVLI ICWGPLLAIM VYDVFGKMNK

  TM7                                      IC4
FGPIFMTIPA FFAKTSAVYN PVIYIMMNKQ FRNCMVTTLC CGKNPLGDST
LIKTVFAFCS MLCLLNSTVN PIIYALRSKD L--------- ----------
```

Figure 5. Sequence alignment of bovine rhodopsin with human CB1R. Residues in black bold are conserved in family A GPCR.

AM251 more than taranabant (7-fold). The origin of this discrepancy became apparent later in the docking studies because W5.43(279)A appeared to be interacting with the variable region of these three molecules (5-Cl-Ph of rimonabant, 4-I-Ph of AM251, and 3-CN-Ph of taranabant). Nonetheless, the mutagenesis data outlined above highlighted the similarity in binding to CB1R between AM251/rimonabant and taranabant. However, it also revealed one significant difference between AM251/rimonabant and taranabant that the S7.39(383)A mutation dramatically impacted the binding of taranabant (202-fold) but not AM251 (2-fold), while the K3.28(192)L mutation significantly affected the binding of AM251/rimonabant (17-fold) but not taranabant (2-fold).

To further understand the binding of taranabant, a CB1R homology model was constructed for docking studies. Like most other GPCRs, no crystal structure of CB1R is available. We took a similar approach to others reported in the literature starting from the crystal structure of bovine rhodopsin.[10] Shown in Figure 5 is the amino acid sequence alignment of human CB1R with bovine rhodopsin.[11] The key conserved residues were labeled in black bold letters, and transmembrane helices were highlighted in yellow. The minimized CB1R homology model is very similar to that of Salo et al.[8e]

Because the mutagenesis data were suggestive of significant overlap between AM251/rimonabant and taranabant in their binding to CB1R, the bioactive conformation of taranabant should resemble that of AM251/rimonabant. The conformation of rimonabant has been well studied.[12] Among the two low-energy conformers (Tg form and Ts form), the Tg conformer (Figure 6) was found to dock better to CB1R.[8b] Various

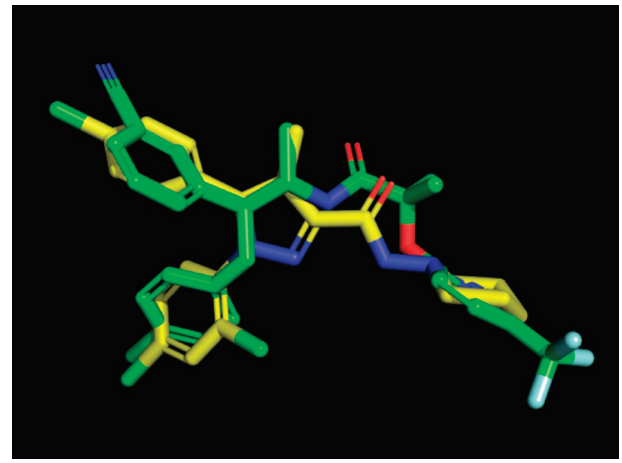

Figure 6. Overlay of conformer D of taranabant (green) with rimonabant (yellow).

conformers of taranabant were evaluated for overlap with rimonabant, and conformer D was deemed the best fit and was selected for docking studies. The minimized binding model of taranabant is presented in Figure 7. Several interactions are noteworthy: (1) the 3-CN-Ph ring resided in a hydrophobic pocket formed by W(5.43)279 and Y(5.39)275 and may be engaged in $\pi-\pi$ stacking with the indole ring of W(5.43)279 and the hydroxyphenyl ring of Y(5.39)275. The cyano group of taranabant and the hydroxyl group of Y(5.39)275 were not positioned perfectly for hydrogen bonding, but the respective electron-withdrawing and electron-donating nature of these two

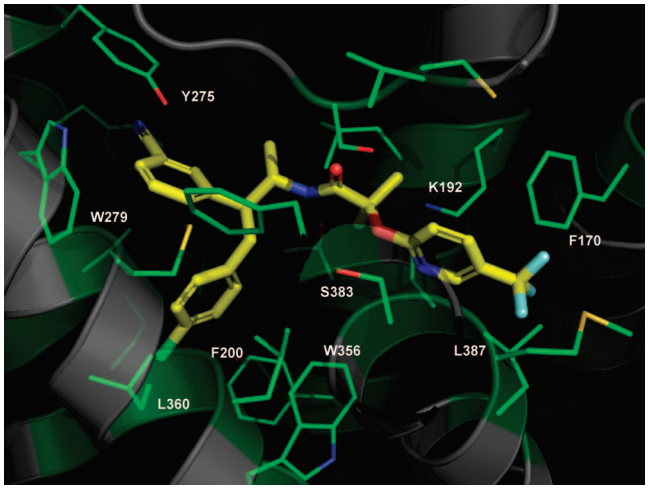

Figure 7. The binding mode of taranabant in the CB1R homology model.

substituents may enhance π-stacking interactions; (2) the 4-Cl-Ph ring resided in another pocket formed by F(3.36)200, W(6.48)356, and L(6.52)360, engaging in π-stacking and hydrophobic interactions; (3) Ser(7.39)383 was located near the amide bond, and the hydroxyl oxygen formed a hydrogen bond with the amide NH of taranabant. This interaction contributed greatly to the binding of taranabant, as reflected by the 200-fold loss of affinity to the Ser(7.39)383A mutant receptor relative to the wild type. The strength of this hydrogen bond may be explained by the high lipophilicity of surrounding residues or hydrophobic enclosure, as described by Friesner;[13] (4) K(3.28)192, previously shown to be critical to the binding to rimonabant, was not appropriately situated to hydrogen bond with taranabant; and (5) the 5-CF_3-Pyr ring was positioned appropriately for π-stacking interactions with F(2.57)170 and hydrophobic interactions with L(7.42)387.

Conclusions

Despite lack of a rigid cyclic core, taranabant was shown by X-ray crystallographic, solution NMR, and computational studies to have a significant degree of conformational rigidity, particularly along the C11−N13−C14−C16−C17 backbone. The preferred conformation both at the solid state and in solution featured staggered substituents along bonds C16−C17 and C14−C16 to avoid nonbonded eclipsing or gauche interactions. Additional conformational restraint was provided by the *trans*-amide bond. In contrast, the C8−C11 and O7−C8 bonds were more freely rotated to allow the CF_3-Pyr ring accessing to various directions.

Mutagenesis and docking studies suggested that taranabant and rimonabant shared a general binding area of CB1R, although the two classes of CB1R inverse agonists differed in detailed interactions. Similar to rimonabant, taranabant interacted with a cluster of aromatic residues (F(3.36)200, W(5.43)279, W(6.48)356, and Y(5.39)275) of CB1R through the two phenyl rings and with F(2.57)170 and L(7.42)387 through the CF_3-Pyr ring. These interactions together likely formed the basis of binding between an inverse agonist ligand and the putative inactive state of CB1R. The unique importance of K(3.28)192 for AM251 and S(7.39)383 for taranabant, each providing a hydrogen bond, highlighted the differences in binding between the two classes of CB1R inverse agonists. These results also suggested that the interaction with K(3.28)192 may not be as critical for stabilizing the putative inactive state of CB1R as previously proposed. Finally, the strong hydrogen bond formed between the NH of taranabant and the hydroxyl of S(7.39)383 was essential to the superior CB1R binding affinity of taranabant.

Experimental Section

Materials. The synthesis of taranabant has been disclosed.[6]

X-ray Crystal Structure Determination. Crystals of taranabant suitable for X-ray analysis were obtained by slow evaporation from methyl-*t*-butyl ether/hexanes (v/v 1:1). Data were collected on a Bruker CCD diffractometer to a θ limit of 26.50°, which yielded 32603 reflections. There are 12217 unique reflections with 6727 observed at the 2σ level. The structure was solved by direct methods (SHELXS-97)[14a] and refined using full-matrix least-squares on F^2 (SHELXL-97).[1b] The final model was refined using 723 parameters and all 12217 data points. One unit cell comprises two independent molecules of the main organic moiety along with a solvent molecule (methyl-*t*-butyl ether). All nonhydrogen atoms were refined with anisotropic thermal displacements. The final agreement statistics are as follows: $R = 0.058$ (based on 6727 reflections with $I > 2\sigma(I)$), $wR = 0.129$, $S = 0.94$ with $(\Delta/\sigma)\text{max} = 0.03$. The maximum peak height in a final difference Fourier map is 0.898 $eÅ^{-3}$, and this peak is without chemical significance; molecular formula, $C_{27}H_{25}C_{l1}F_3N_3O_2$, $C_5H_{12}O$; M*r* = 1120.057; monoclinic, $P2_1$; a = 10.156(3), b = 25.682(9), c = 11.369(4) Å, β = 90.845(7)°, V = 2965.2(17) $Å^3$, Z = 2, Dx = 1.254 gcm^{-3}; monochromatized radiation λ(Mo) = 0.71073 Å, μ = 0.18 mm^{-1}, $F(000)$ = 1172, T = 100 K.[15] The final Flack parameter is 0.07(9).

NMR Spectroscopy. The NMR spectra of taranabant were recorded at 600 MHz using a Varian Inova spectrometer in CD_3OD as a solvent at 25 °C.[16] Signal assignments were confirmed by 2D COSY and HSQC NMR experiments. NOE data were recorded using 2D NOESY with mixing times of 0.4, 0.8, and 1.2 s.

Molecular Modeling and Docking. All calculations were performed on a Linux work station. The initial structure of taranabant was constructed and further minimized using the MMFF force field and charge set to yield a suitable starting point for the generation of multiple conformers.[17] With the jg routine in MIX environment developed in-house,[18] about 100 conformers were generated with energies ranging within 12 kcal/mol. The jg command created multiple geometric configurations using distance geometry and relied on the atom information of the molecule for construction of geometric restraints. During the generation process, the chirality of the conformers was fixed as (*S*,*S*). The geometry of each conformer was further minimized with the batchmin routine. After minimization, the conformers were checked against one another based on energy and rms differences, and each unique conformer was saved.

The CB1 receptor homology model was generated from the crystal structure of bovine rhodopsin, with the homology module in MOE program of CCG computing.[19] A local energy minimization was carried out first for the regions of gap and insertion. A global minimization was followed to relieve the steric repulsions, while C_α of the *trans*-membrane helices were constrained so that the backbones of the TM region remain unchanged. The loops were further refined with the high temperature molecular dynamics simulations with Charmm.[20] A distance-dependent dielectric constant was used because the MD simulation was mainly for the extracellular loops under a hydrophilic environment. A femtosecond step integration time was used for the simulation. The conformer of interest was docked and scored by the scoring scheme that counted the overlapping of the spheres and the atoms of the ligand. The binding site was defined as 12 Å around Lys192, and only the polar hydrogens of the receptor were present during the docking process.

Site-Directed Mutagenesis. pCDNA3-h CB1R, containing all the coding region of human CB1 receptor, was a gift from Dr. Gary O'Neill (Merck Research Laboratories, Montreal). Mutant human CB1 receptors were generated by site-directed mutagenesis using GeneEditor (Promega, Cat: Q9280), with the following mutagenesis primers:

F170L: 5′-CTGGGGAGTGTCATTTTAGTCTACAGCTTCATTG-3′

K192L: 5′-CGCAACGTGTTTCTGTTCTTACTGGGTGGGGTCACG-3′

F200A 5′-GGGGTCACGGCCTCCGCCACTGCCTCCGTGGGC-3′

W279A: 5′-ACCTACCTGATGTTCGCGATCGGGGTCACCAGC-3′

S383A: 5′- GTGTTTGCATTCTGCGCTATGCTCTGCCTGCTG-3″

The identity of the mutant was determined by sequencing the whole coding region. The confirmed coding regions of wild type and mutant human CB1R were cloned into pCDNA5/FRT expression vector.

Cell Culture. CHO (Flp-In, Invitrogen) cells were kept in F12 medium with 10% dialyzed fetal bovine serum, 1× ITS-A (Invitrogen, Cat.: 51300-044), 2 mM L-glutamine, 1× penicillin-streptomycin, and 100 μg/mL zeocin. Transfections were done in six-well plate with Lipofectamine 2000 (Invitrogen, Cat.: 11668-027). At 24 h after transfection, CHO cells were transferred to T75 with selective medium (F12 medium with 10% dialyzed-FGS, 1× ITS-A, 2 mM L-glutamine, 1× penicillin-streptomycin, and 600 μg/mL hygromycin B). Stable clones were isolated by limited dilution.

CHO cells were harvested by enzyme-free dissociation buffer (GIBCO), the cells were spun down at 220× g by a Beckman table top centrifuge for 10 min, and the pellet was resuspended in membrane homogenizing buffer (10 mM Tris, pH 7.2, 1 mM EDTA, and protease inhibitor cocktails from SIGMA P8340). Cells were homogenized with motor-driven homogenizer (Talboy setting 30), 10 strokes, and then spun in 50 mL conical tubes at 690× g for 10 min in a Beckman table top centrifuge. Supernatants were transferred to centrifuge tubes and spun at 38724× g for 20 min. The pellet membrane fraction was resuspended in membrane storage buffer (50 mM Tris, pH 7.2, 2.5 mM EDTA, 5 mM $MgCl_2$, 100 g/L sucrose, plus protease inhibitor cocktails). The resulting membrane solution was frozen in liquid nitrogen and was stored at −80 °C.

Radio-Labeled Binding Assay. Equilibrium binding assays were performed by incubating human CB1R CHO membranes, test compound and 0.5 nM [^{3}H]-CP55940, or 1 nM [^{3}H]-SR141716A in the binding buffer (50 mM Tris-HCl, pH 7.2, 2.5 mM EDTA, 5 mM $MgCl_2$, 0.05% fatty acid free BSA, 1× protease inhibitor cocktail, from Sigma P8340) at 37 °C for 1 h. GF/C filter (MAHF C1H 60 FC plate, Millipore) was prewetted with wash buffer (binding buffer without protease inhibitor). The binding reaction was terminated by filtering the binding solution through GF/C filter with a Packard harvester, and the filters were washed with 1 mL of wash buffer per well six times. After drying, 50 μL of Microscint 20 was added, the plate was sealed, and the radioactivity of bound [^{3}H]-CP55940 or [^{3}H]-SR141716A was counted on a Packard Topcount. Binding IC_{50}s were determined by one site-competition curve-fitting method with PRISM (version 4, GraphPad Software, Inc.) software.

Acknowledgment. We gratefully acknowledge Prof. O. M. H. Salo for sharing the coordinates of his human CB1R homology model.

Supporting Information Available: Annotated 1D ^{1}H NMR, 2D ^{1}H−^{1}H NOESY NMR, 2D^1 H−^{13}C HSQC NMR, and 2D^1 H−^{1}H COSY NMR spectra of taranabant. This material is available free of charge via the Internet at http://pubs.acs.org.

References

(1) (a) Greenberg, I.; Kuehnle, J.; Medelson, J.; Bernstein, J. Effects of marijuana use on body weight and caloric intake in humans. *Psychopharmacology* **1976**, *49*, 79–84. (b) Trojniar, W.; Wise, R. A. Facilitory effect of Δ9-tetrahydrocannabinol on hypothalamically induced feeding. *Psychopharmacology* **1991**, *103*, 172–176.

(2) (a) Arnone, M.; Maruani, J.; Chaperon, F.; Thiebot, M.; Poncelet, M.; Soubrie, P.; Le Fur, G. Selective inhibition of sucrose and ethanol intake by SR141716, an antagonist of central cannabinoid (CB1) receptors. *Psychopharmacology* **1997**, *132*, 104–106. (b) Simiad, J.; Keane, M.; Keane, P. E.; Soubrie, P. SR141716, a CB1 cannabinoid receptor antagonist, selectively reduces sweet food intake in marmoset. *Behav. Pharmacol.* **1998**, *9*, 179–181. (c) Blundell, J. E.; Jebb, S. A.; Stiubbs, R. J.; Wilding, J. R.; Lawton, C. L.; Browning, L.; Whybrow, S.; Halford, J. C. G. Effect of rimonabant on energy intake, motivation to eat and body weight with or without hypocaloric diet: the REBA study. *Obesity Rev.* **2006**, *7* (Suppl 2), 104–104. (d) Stevens, C.; Cilissen, C.; Desmet, M.; et al. MK-0364, a CB1R inverse agonist, reduces acute food intake in overweight/obese male volunteers. *Diabetes* **2007**, *56* (Suppl 1), A462.

(3) (a) Liu, Y. L.; Connoley, I. P.; Wilson, C. A.; Stock, M. J. Effects of the cannabinoid CB1 receptor antagonist SR141716 on oxygen consumption and soleus muscle glucose uptake in Lep(ob)/Lep(ob) mice. *Int. J. Obesity* **2005**, *29*, 183–187. (b) Addy, C.; Heymsfield, S.; Cilissen, C.; et al. MK-0364, a novel CB1R inverse agonist, increases energy expenditure in overweight and moderately obese subjects. *Diabetes* **2007**, *56* (Suppl 1), A461.

(4) (a) Colombo, G.; Agabio, R.; Diaz, G.; Lobina, C.; Reali, R.; Gessa, G. L. Appetite suppression and weight loss after the cannabinoid antagonist SR141716. *Life Sci.* **1998**, *63*, 113–117. (b) Van Gaal, L. F.; Rissanen, A. M.; Scheen, A. J.; Ziegler, O.; Rossner, S. for the RIO-Europe Study Group. Effects of the cannabinoid-1 receptor blockade rimonabant on weight reduction and cardiovascular risk factors in overweight patients: 1-year experience from the RIO-Europe study. *Lancet* **2005**, *365*, 1389–1397.

(5) (a) For recent reviews, see: Antel, J.; Gregory, P. C.; Nordheim, U. CB1 cannabinoid receptor antagonists for treatment of obesity and prevention of comorbid metabolic disorders. *J. Med. Chem.* **2006**, *49*, 4008–4016. (b) Lange, J. H. M.; Kruse, C. G. Medicinal chemistry strategies to CB_1 cannabinoid receptor antagonists. *Drug Discovery Today* **2005**, *10*, 693–702.

(6) (a) Lin, L. S.; Lanza, T. J.; Jewell, J. P.; Liu, P.; Shah, S. K.; Qi, H.; Tong, X.; Wang, J.; Xu, S.; Fong, T. M.; Shen, C.-P.; Lao, J.; Chen, J.; Shearman, L. P.; Stribling, D. S.; Rosko, K.; Strack, A.; Marsh, D. J.; Feng, Y.; Kumar, S.; Samuel, K.; Yin, W.; Van der Ploeg, L.; Goulet, M. T.; Hagmann, W. K. Discovery of *N*-[(1*S*,2*S*)-3-(4-chlorophenyl)-2-(3-cyanophenyl)-1-methylpropyl]-2-methyl-2-{[5-(trifluoromethyl)pyridin-2-yl]oxy}propanamide (MK-0364), a novel, acyclic cannabinoid-1 receptor inverse agonist for the treatment of obesity. *J. Med. Chem.* **2006**, *49*, 7584–7587. (b) Chen, C.-y.; Frey, L. F.; Shultz, S.; Wallace, D. J.; Marcantonio, K.; Payack, J. F.; Vazquez, E.; Springfield, S. A.; Zhou, G.; Liu, P.; Kieczykowski, G. R.; Chen, A. M.; Phenix, B. D.; Singh, U.; Strine, J.; Izzo, B.; Krska, S. W. Catalytic, enantioselective synthesis of taranabant, a novel, acyclic cannabinoid-1 receptor inverse agonist for the treatment of obesity. *Org. Process Res. Dev.* **2007**, *11*, 616–623.

(7) Fong, T. M.; Guan, X.-M.; Marsh, D. J.; Shen, C.-P.; Stribling, D S.; Rosko, K. M.; Lao, J.; Yu, H.; Feng, Y.; Xiao, J. C.; Van der Ploeg, L. H. T.; Goulet, M. T.; Hagmann, W. K.; Lin, L. S.; Lanza, T. J., Jr.; Jewell, J. P.; Liu, P.; Shah, S. K.; Qi, H.; Tong; X.; Wang, J.; Xu, S. S.; Francis, B.; Strack, A. M.; Macintyre, D. E.; Shearman, L. P. Antiobesity efficacy of a novel cannabinoid-1 receptor inverse agonist, *N*-[(1*S*,2*S*)-3-(4-chlorophenyl)-2-(3-cyanophenyl)-1-methylpropyl]-2-methyl-2-{[5-(trifluoromethyl)pyridin-2-yl]oxy}propanamide (MK-0364), in rodents. *J. Pharmacol. Exp. Ther.* **2007**, *321*, 1013–1022.

(8) (a) Kapur, A.; Hurst, D. P.; Fleischer, D.; Whitnell, R.; Thakur, G. A.; Makriyannis, A.; Reggio, P. H.; Abood, M. E. Mutation studies of Ser7.39 and Ser2.60 in the human CB1 cannabinoid receptor: Evidence for a serine-induced bend in CB1 transmembrane helix 7. *Mol. Pharmacol.* **2007**, *71*, 1512–1524. (b) Hurst, D.; Umejiego, U.; Lynch, D.; Seltzman, H.; Hyatt, S.; Roche, M.; McAllister, S.; Fleischer, D.; Kapur, A.; Abood, M.; Shi, S.; Jones, J.; Lewis, D.; Reggio, P. Biarylpyrazole inverse agonists at the cannabinoid CB1 receptor: Importance of the C-3 carboxamide oxygen/lysine3.28(192) interaction. *J. Med. Chem.* **2006**, *49*, 5969–5987. (c) McAllister, S. D.; Rizvi, G.; Anavi-Goffer, S.; Hurst, D. P.; Barnett-Norris, J.; Lynch, D. L.; Reggio, P. H.; Abood, M. E. An aromatic microdomain at the cannabinoid CB(1) receptor constitutes an agonist/inverse agonist binding region. *J. Med. Chem.* **2003**, *46*, 5139–5152. (d) Hurst, D. P.; Lynch, D. L.; Barnett-Norris, J.; Hyatt, S. M.; Seltzman, H. H.; Zhong, M.; Song, Z. H.; Nie, J.; Lewis, D.; Reggio, P. H. *N*-(Piperidin-1-yl)-5-(4-chlorophenyl)-1-(2,4-dichlorophenyl)-4-methyl-1*H*-pyrazole-3-carboxamide (SR141716A) interaction with LYS3.28(192) is crucial for its inverse agonism at the cannabinoid CB1 receptor. *Mol. Pharmacol.* **2002**, *62*, 1274–1287. (e) Salo, O. M. H.; Lahtela-Kakkonen, M.; Gynther, J.; Jarvinen, T.; Poso, A. Development of a 3D model for the human cannabinoid CB1 receptor. *J. Med. Chem.* **2004**, *47*, 3048–3057. (f) Shen, C.-P.; Xiao, J. C.; Armstrong, H.; Hagmann, W. K.; Fong, T. M. F200A substitution in the third transmembrane helix of human cannabinoid CB1 receptor converts AM2233 from receptor agonist to inverse agonist. *Eur. J. Pharmacol.* **2006**, *15*, 41–46.

(9) Lange, J. H. M.; Coolen, H. K. A. C.; van Stuivenberg, H. H.; Dijksman, J. A. R.; Herremans, A. H. J.; Ronken, E.; Keizer, H. G.; Tipker, K.; McCreary, A. C.; Veerman, W.; Wals, H. C.; Stork, B.; Verveer, P. C.; den Hartog, A. P.; de Jong, N. M. J.; Adolfs, T. J. P.; Hoogendoorn, J.; Kruse, C. G. Synthesis, biological properties, and molecular modeling investigations of novel 3,4-diarylpyrazolines as potent and selective CB_1 cannabinoid receptor antagonists. *J. Med. Chem.* **2004**, *47*, 627–643.

(10) Palczewski, K.; Kumasaka, T.; Hori, T.; Behnke, C. B.; Motoshima, H.; Fox, B. A.; Le Trong, I.; Teller, D. C.; Okada, T.; Stenkamp, R. E.; Yamamoto, M.; Miyano, M. Crystal structure of rhodopsin: A G protein-coupled receptor. *Science* **2000**, *239*, 739–745.

(11) (a) Ballesteros, J.; Palczewski, K. G protein-coupled receptor drug discovery: Implications from the crystal structure of rhodopsin. *Curr. Opin. Drug Discovery Dev.* **2001**, *4*, 561–574. (b) Baldwin, J. M.; Schertler, G. F.; Unger, V. M. An alpha-carbon template for the transmembrane helices in the rhodopsin family of G-protein-coupled receptors. *J. Mol. Biol.* **1997**, *272*, 144–164.

(12) Shim, J.-Y.; Welsh, W. J.; Cartier, E.; Edwards, J. L.; Howlett, A. C. Molecular interaction of the antagonist *N*-(piperidin-1-yl)-5-(4-chlorophenyl)-1-(2,4-dichlorophenyl)-4-methyl-1*H*-pyrazole-3-carboxamide with the CB1 cannabinoid receptor. *J. Med. Chem.* **2002**, *45*, 1447–1459.

(13) Friesner, R. A.; Murphy, R. B.; Repasky, M. P.; Frye, L. L.; Greenwood, J. R.; Halgren, T. A.; Sanschagrin, P. C.; Mainz, D. T. Extra precision glide: Docking and scoring incorporating a model of hydrophobic enclosure for protein−ligand complexes. *J. Med. Chem.* **2006**, *49*, 6177–6196.

(14) (a) Sheldrick, G. M. Phase annealing in SHELX-90: Direct methods for larger structures. *Acta Crystallogr.* **1990**, *A46*, 467–473. (b) Sheldrick, G. M. *SHELXL-97*, Program for the refinement of crystal structures; Univ. of Göttingen, Germany.

(15) CCDC 632855 contains the supplementary crystallographic data for this paper, which can be obtained free of charge from The Cambridge Crystallographic Data Centre via http://www.ccdc.cam.ac.uk/data_request/cif.

(16) Annotated spectra are included in the Supporting Information.

(17) Halgren, T. A. MMFF VII. Characterization of MMFF94, MMFF94s, and other widely available force fields for conformational energies and for intermolecular-interaction energies and geometries. *J. Comput. Chem.* **1999**, *20*, 730–748.

(18) Underwood, D. J.; Sheridan, R. P.; Miller, M. D. Flexibases: A way to enhance the use of molecular docking methods. *J. Comp.-Aided Mol. Des.* **1994**, *8*, 565–582.

(19) Labute, P. Chemical Computing Group Inc., MOE deployment strategies, http://www.chemcomp.com/software-pro.htm, accessed on Oct. 26, 2007.

(20) Brooks, B. R.; Bruccoleri, R.; Olafson, B. D.; States, D. J.; Swaminathan, S.; Karplus, M. CHARMM: A program for macromolecular energy, minimization, and dynamics calculations. *J. Comput. Chem.* **1983**, *4*, 187–217.

JM7014974